DESIGN OF THE BOOSTER SYNCHROTRON MAGNET FOR JAPANESE 12 GEV PROTON SYNCHROTRON

H. Sasaki, K. Takikawa and M. Kumada
National Laboratory for High Energy Physics
Ibaraki, Japan

Abstract

A booster synchrotron for 12 GeV proton synchrotron is under construction. Specially developed oriented steel is proposed for the core material of the magnet of the high repetition booster synchrotron. Present material shows good high-field characteristics, low loss and low coercive force. The data of the electro-magnetic and mechanical properties of this material are presented in comparison with those of ordinary silicon steel. The results of the calculation of the magnetic field are shown and discussed.

I. Introduction

Fast-cycling electron or proton synchrotron magnets have been designed and constructed with ordinary transformer silicon steel with few exceptions. In the industrial field, however, oriented silicon steel has been currently applied to the construction of transformers, reactors and generators, and this fact results in the reduction of the core weight and the improvement of the electromagnetic properties of those machines. On the other hand, the extensive studies of the application of the oriented steel to slow-cycling pulsed magnet for proton synchrotron were made, and good results were obtained.[1] Especially, due to the high permeability in the orientation direction of the core material, the high field behaviours in the magnet gap showed remarkable improvements to the saturation effects with the roll direction perpendicular to the median plane.

In the design of the magnet of a 500 MeV fast-cycling booster synchrotron, the magnetic bending radius has to be obtained by minimizing the sum of the costs of the magnet, its power supply and the building for them. This leads to a relatively high maximum field, say, 13 kG to 14 kG. This field is too high to maintain a good field distribution in the useful region of the magnet gap without any field-correction devices. With the magnetic characteristics of the core material, therefore, the maximum field should be chosen to be as high as possible within the tolerances of the magnetic field distribution at the maximum excitation.

In most cases of fast-cycling synchrotron magnets, their maximum central field is designed to several kilogauss with ordinary silicon steel. The saturation induction of the silicon steel tends to lower its value with silicon content, e.g., 21.5 kG for pure iron, 19.7 kG for 4 % silicon steel. Oriented low-silicon steel of 1 mm in thickness, which was developed for slow-cycling pulsed magnets of a proton synchrotron, showed a high saturation induction, 21 kG, and high permeabilities at high field region. From these considerations, oriented low-carbon and low-silicon steel of 0.35 mm in thickness newly developed was chosen for the fast-cycling 500 MeV booster synchrotron magnet as the core material. In the application of such material to the fast-cycling magnet, of course, the power dissipation, sheet-handling at punching and fabrication procedures, cost, etc., should be taken into consideration in addition to the electromagnetic properties of the material.

The parameters of the booster synchrotron magnet are collected in Table 1.

Table 1. Parameters of the booster synchrotron magnet

max. energy (max. magnetic field)	500 MeV (11.018 kG)
injection energy (injection field)	20 MeV (1.969 kG)
radius of curvature	3.3 m
mean radius	6.0 m
number of magnet units (containing an additional dummy magnet)	9
profile parameter	3.664 m^{-1}
lattice structure	FDFO
length of D-sector	1.2824 m
length of F-sector	0.6547 m x 2
gap of magnet at central orbit	7.6 cm
vertical semi-aperture of vac. chamber	3.0 cm
horizontal semi-aperture of vac. chamber	7.0 cm
repetition rate	20 Hz

II. Mechanical and electro-magnetic properties of the oriented steel

The proposed steel is a killed, singly grain-oriented steel supplied from Kawasaki Steel Corporation in Japan. The chemical composition of the material is shown in Table 2. From the table, it can be seen that carbon and silicon contents are of considerably small amount in comparison with ordinary silicon steel. From the view point of the high saturation induction, it is desirable that oriented iron is as pure as possible, but pure iron

Table 2. Chemical composition of the oriented steel

element	C	Si	Mn	P	S	Al(sol.)	Co
weight percent	0.001	0.83	0.056	0.006	0.008	0.002	0.005

Table 3. Mechanical properties of the oriented steel

density (g/cm^3)	thickness (mm)	space factor (%)	hardness (HV 1kg)		yield point (kg/mm^2)	tensile strength (kg/mm^2)	elongation (%)
7.80	0.355	98.9	104	L*	13.7	21.0	30.8
				C	14.3	21.9	100.0

* L: roll direction C: crosswise direction to rolling

is costly and is too soft to fabricate magnet core. Addition of a small amount of silicon gives the material an appropriate hardness and increases the specific resistance of the material, maintaining the high saturation induction of pure iron. The mechanical properties of the material are summarized in Table 3. Some differences can be found in the mechanical properties between in the roll direction and in the crosswise direction to rolling. As a whole, these properties are inferior to those of ordinary silicon steel, e.g., by half in hardness and by two-third in yield point.

The electro-magnetic properties of the proposed oriented steel are collected in Table 4 in comparison with those of an ordinary high-grade silicon steel RM9, which is in production by Kawasaki Steel Corporation. In spite of low

Table 4. Electro-magnetic properties of the oriented steel and ordinary high-grade silicon steel RM9

		RM9	Proposed oriented steel L	Proposed oriented steel C
thickness (mm)		0.35	0.35	
density (g/cm^3)		7.65	7.80	
specific resistance ($\mu\Omega\cdot cm$)		49.0	20.2	
interlamination resistivity ($\Omega\cdot cm^2$/sheet)		13	13	
iron loss (W/kg)	$W_{10/50}$	0.90	1.10	1.54
	$W_{15/50}$	2.20	2.30	4.10
dc flux density (kG)	$B_{0.8}$	7.4	13.0	6.7
	$B_{2.4}$	12.2	17.2	11.6
	B_4	13.1	18.0	12.8
	B_8	13.7	18.8	13.8
	B_{20}	14.9	19.8	14.9
	B_{40}	15.9	20.4	15.6
	B_{80}	17.0	20.7	16.6
max. permeability		9,900	24,000	8,800
permeability		703 at 15 kG	810 at 20 kG	203 at 16.5 kG
coercive force (Oe)		0.28 at 15 kG	0.22 at 18 kG	0.37 at 16.5 kG
remanent flux density (kG)		6.9	12.2	7.8

specific resistance of the oriented steel, iron loss of the material in the magnetization at 50 Hz in roll direction is comparable to the loss of the silicon steel. On the other hand, the oriented steel magnetized crosswisely to roll direction shows high iron losses corresponding to those of low-grade silicon steel.

Above all, the proposed oriented steel is remarkably characterized by the magnetization curves as shown in Fig.1. Namely, the high field characteristics of the oriented steel are extremely superior in the direction of the magnetization parallel to the roll direction, e.g., the permeability at 20 kG is as high as 800. In other words, the magnetic induction, which gives such a high per-

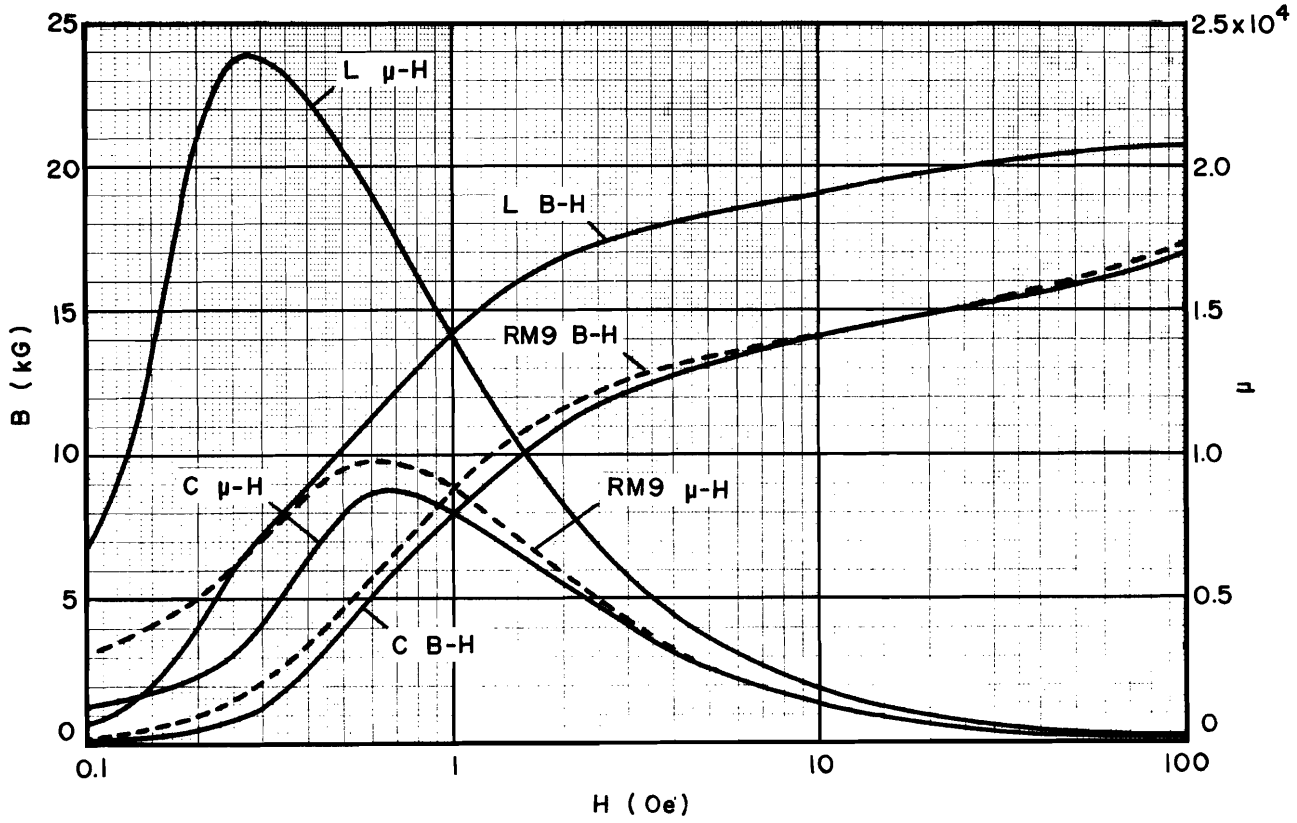

Fig.1 Magnetization curves of the proposed oriented steel and an ordinary silicon steel RM9 in dc excitation. L and C denote the magnetization in the roll direction and in the crosswise direction to rolling, respectively.

meability, is by an amount of 5 kG higher than that of the ordinary silicon steel. This fact means that we can raise the maximum induction on the central orbit in the magnet gap by about 3 kG without any additional field distortions in comparison with the ordinary silicon steel. Even in the crosswise direction to rolling, the oriented steel shows the same behaviour as the high-grade silicon steel at high field region. The directional dependence of the magnetization is shown in Fig.2. In this figure, it can be found that the magnetization in the irreversible magnetization region is difficult at an angle of 55° from the roll direction. This is explained by a Goss texture of the crystalline structure of the material.

The coercive force of the proposed oriented steel is considerably low in the roll direction, and even in the crosswise direction it is comparable to that of high-grade silicon steel. Low coercive force is preferable in the view points of the field-errors at injection and of the power dissipation in the magnet core. However, the coercive force depends on the excitation conditions such as the maximum induction, excitation frequency, stress in the core material, etc. Fig.3 shows dynamic hysteresis loops of the present material at various frequencies. The stress, which is introduced into the core material at the curing stage of adhesive resin, brings about the change of the coercive force.[2] The amount of the variation of the coercive force depends on the geometrical conditions of the stacked block, the curing conditions, the mechanical properties of the adhesive resin, etc. The dependence of the coercive force on the stress in the core material is very complex. However, such a problem will be resolved by an appropriate choice of the resin.

III. General design of the magnet

The booster synchrotron magnet consists of a ring shaped structure with 12 m in diameter. This structure comprises 8 magnet units, each composed of a defocusing sector sandwiched by focusing half-sectors. Each magnet unit is divided into 14 adjacent magnet blocks. The block is formed by cementing the laminations of the oriented steel by epoxy-resin in a fan shape with 3.3 m radius of curvature at the central orbit. The stacking factor of 90 % is expected to be attainable. The fabrication accuracy of the pole profile is within 0.05 mm. The end blocks will be specially shaped to reduce eddy-current heating and the variation of the effective magnetic length with excitation. The core blocks are assembled each other by means of adequate combining jigs and a steel cover-plate, and they are mounted on a steel girder, which is equipped with leveling and translating devices. The cross-sectional view of the magnet is shown in

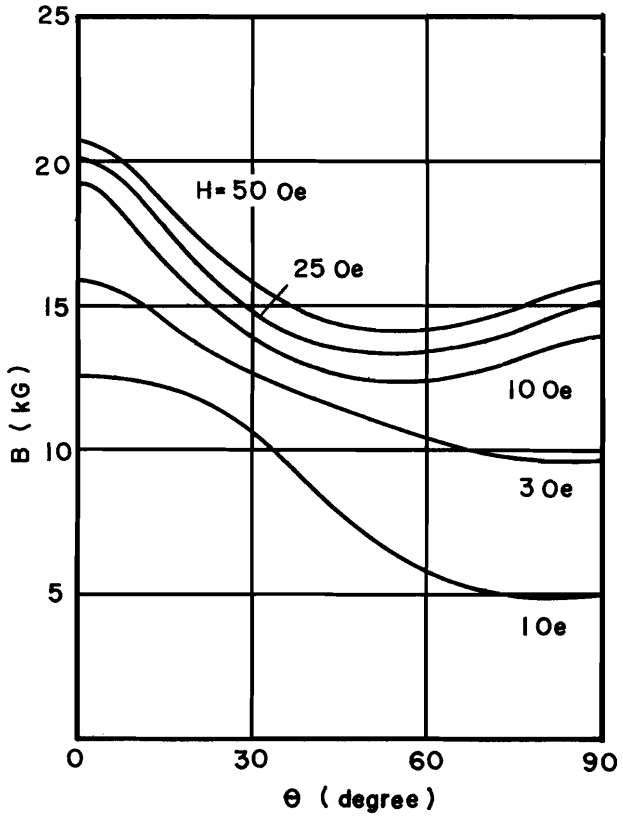

Fig.2 Directional dependence of magnetization of the oriented steel. θ is the angle from the roll direction.

Fig.4.

Hollow water-cooled copper conductor is proposed for the magnet windings. Both solid and stranded copper conductors have been considered. Application of stranded copper cables would depress the eddy current power dissipation to negligible amounts. However, it is inevitable that the mechanical structure of the windings involving water-cooling devices is complicated, and this fact leads to high cost of the windings. On the other hand, although the power dissipation of solid conductor due to eddy current in the operation at 20 Hz is appreciable, it can be reduced to some extent by an adequate procedure of the coil fabrication. Namely, the cross-sectional area of the solid conductor required to carry the total current is divided into two parts, which are connected in parallel to each other. These parallel conductors are transposed at the connection points between pancakes and are short-circuited electrically at the input and output terminals of the windings. Such a procedure of the connection of the windings will reduce the power dissipation due to the eddy currents in the solid conductors to about one-third in present estimates.

The coil windings are impregnated with epoxy-resin in vacuum.

From the feature of high-repetition operation and of large amounts of the stored magnetic energy, a multisection series-resonant network proposed by White et al.[3] is adopted to the excitation of the magnet. The configuration of the resonant magnet network is a simple 3-mesh resonant network, each group containing three series-connected magnet units, resonant capacitor and the winding of energy-storage choke. The magnet network consists of nine magnet units involving an auxiliary dummy magnet.

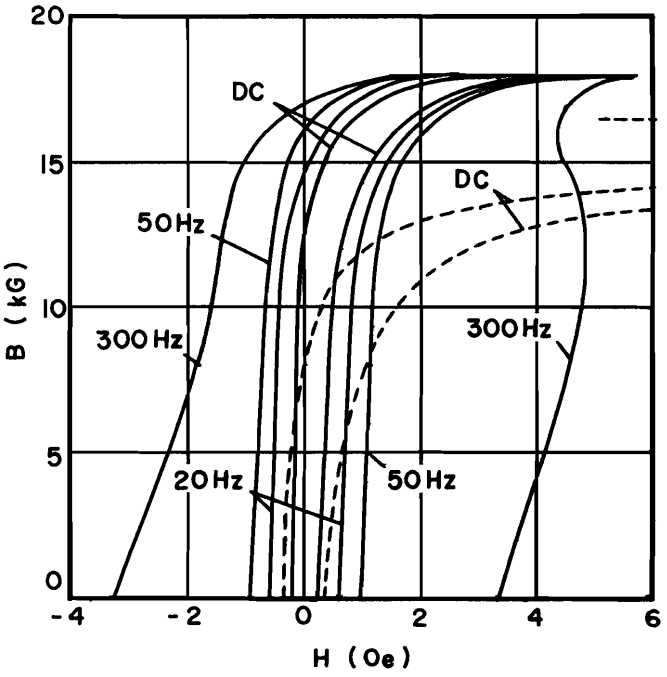

Fig.3 Dynamic hysteresis loops of the oriented steel. Solid curve is the magnetization with the maximum flux density of 18 kG in the roll direction, and dashed curve the magnetization with 16.5 kG in the cross-wise direction.

For the central ac power supply, a pulse power supply circuit will be used. Such a type of ac power supply is successfully operating at CEA and Nina. In our power supply, grid-controlled mercury-arc tubes for the pulse- and rectifier- tubes will be replaced by thyristors.

The bias current will be also provided by a rectifier set using thyristors.

IV. Design of the pole profile

The booster magnet must provide a good field over the full aperture through the acceleration stage. The criterion for the good field is that the field gradients are kept constant within 0.5 % over the full width of 13 cm at all excitation levels from the injection field of 2 kG to the

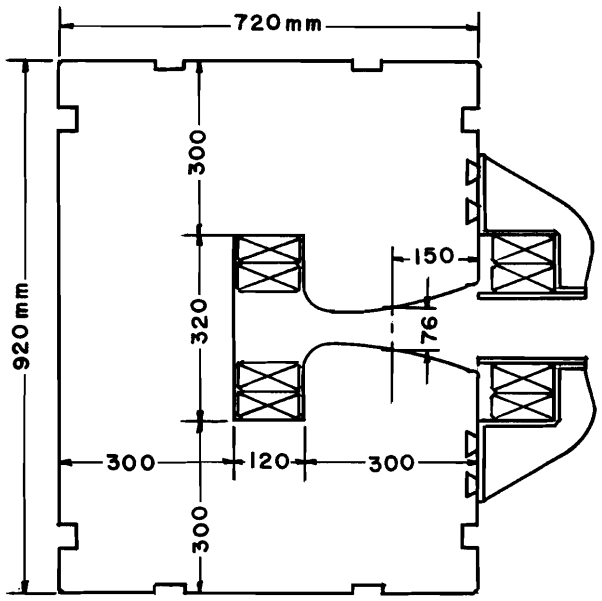

Fig.4 Cross-sectional view of the booster magnet.

maximum field of 11 kG. This is rather stringent requirements for fast-cycling magnet. Owing to high injection field, however, the deviations from the designed field at the beginning of the cycle, which might be brought about by coercive force and low initial permeability, are expected sufficiently small. Therefore, the efforts on the establishment of linear fields were concentrated on obtaining the minimum pole width against decreasing permeabilities due to the saturation.

The lack of symmetry between the open and the closed region of the pole piece might make one to tempt to use asymmetrical pole pieces. This scheme would lead to breaks in the continuous alignment of the vertical pole faces at the boundaries of the focusing and defocusing sectors, which would provide any hindrances for the alignment of magnet blocks and for the fabrication of the magnet coils. It was therefore decided to have symmetrical pole pieces.

An extensive survey on the application of oriented steel to gradient synchrotron magnet has been done.[1] From the results of this survey, we can draw the following conclusions on the design of the pole profile:

1. If the gradient magnet is made of oriented steel with the orientation direction perpendicular to the median plane of the magnet gap, a high quality magnetic field distribution in the gap is achievable in the region of high flux density.

2. The field quality in the magnet gap is mainly determined by the magnetic properties of the pole material in the direction perpendicular to the median plane. The field gradient distribution can be estimated with a good accuracy by the computer calculation assuming that the magnetic properties are isotropic and that permeabilities are those in the roll direction.

Of course, it is desirable to take the directional dependence of the permeability as shown in Fig.2 into consideration at the calculation of the fields. Since in the present stage, we have no means to make such a procedure in the field calculation[4], we have followed the procedure assigned by the conclusion 2.

The design parameters of the pole profile are listed in Table 5. Fig.5 shows the geometrical details of the designed pole profile. The field calculation of the maximum excitation was done on the two cases of B-μ curves as shown in Fig.6; one is the average B-μ curve of the supplied material, whose permeability at 20 kG is 800 in the roll direction, another one the B-μ curve applied to the preliminary studies, which is corresponding to the lower limit of the B-μ curve of the supplied material, i.e., the permeability at 20 kG is as high as 400. The results of the field calculations are shown in Fig.7, and it can be seen that our requirements on the field quality are sufficiently fulfilled. In the real operation of the magnet, however, the trajectories of the operation point in the B-H plane are not necessarily in coincidence with the initial B-μ curve as assigned in the field calculations. Moreover, the magnet is operated dynamically with dc biasing field, and each point in the material must follow different minor loops. These facts will lead to the lowering of the effective permeabilities and of the field qualities. Those problems must await trials on the real operation of magnet to estimate the deviation from the designed field distribution.

Table 5. Design parameters of the pole profile

	F-sector		D-sector
gap height		7.6 cm	
pole width		30 cm	
k_0	3.66407 m^{-1}		-3.66407 m^{-1}
sextupole component	-0.615 m^{-2}		-0.934 m^{-2}
useful horizontal semi-aperture		6.5 cm	

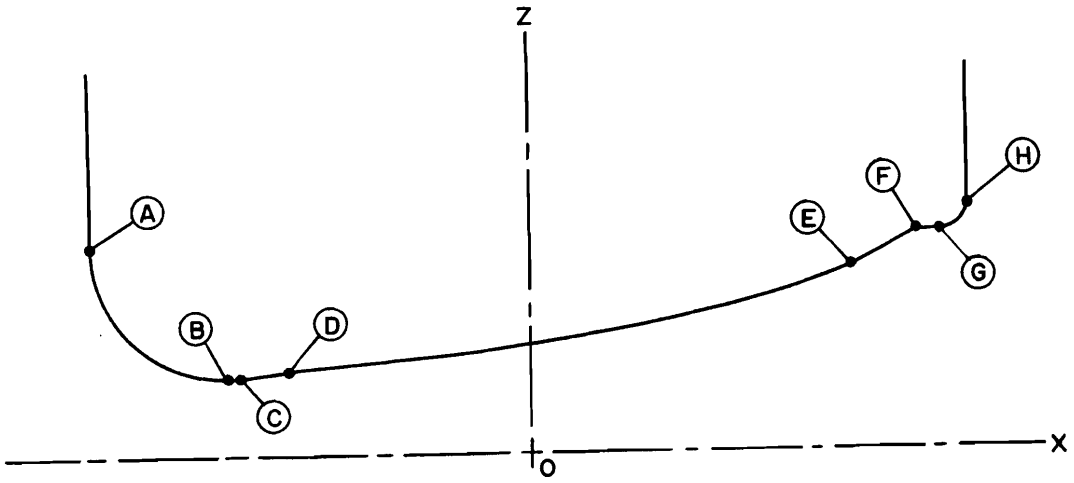

	F-sector			D-sector		
	x	z		x	z	
A	150	73.180	$(x-104)^2+(z-73.180)^2=46^2$	-150	73.210	$(x+104)^2+(z-73.210)^2=46^2$
B	104	27.180	$z=27.180$	-104	27.210	$z=27.210$
C	100	27.180	$(x-100)/17 =-(z-27.180)/2.004$	-100	27.210	$(x+100)/17=(z-27.210)/2.008$
D	83	29.184	$z(1+k_1x+\frac{1}{2}k_2x^2)-\frac{1}{6}(\frac{k_1}{\rho}+k_2)z^3$ $=z_0-\frac{1}{6}(\frac{k_1}{\rho}+k_2)z_0^3$ $k_1=3.66407\times10^{-3}$ $k_2=-0.615\times10^{-6}$ $\rho=3.3\times10^3$ $z_0=38$	-83	29.218	$k_1=-3.66407\times10^{-3}$ $k_2=-0.934\times10^{-6}$ $\rho=3.3\times10^3$ $z_0=38$
E				110	64.144	$(x-110)/22=(z-64.144)/11.766$
F	-130.5	73.613	$z=73.613$	132	75.910	$z=75.910$
G	-140	73.613	$(x+140)^2+(z-83.613)^2=10^2$	140	75.910	$(x-140)^2+(z-85.910)^2=10^2$
H	-150	83.613		150	85.910	

Fig.5. Pole profile of the booster magnet. Dimensions are in mm.

V. Field errors introduced by the statistical fluctuation of magnetic properties of the core material

The statistical fluctuation of the permeability at high field region

At high field, the field errors along the orbit mainly come from the fluctuation of the permeability. The permeability of the supplied material from the manufacturer fluctuates with the standard deviation of 24.4 % at 20 kG in the roll direction and of 5.0 % at 16.5 kG in the crosswise direction to rolling, respectively. Although the permeability in the roll direction at high field spreads over a wide range, its contribution to the variation of the flux density in the magnet core is negligible, because of high permeability. Namely, the average permeability $\bar{\mu}$ in the magnet core is expressed by

$$\ell/\bar{\mu} = \ell_L/\mu_L + \ell_C/\mu_C \ ,$$

where ℓ is the total path length along the magnetic flux line in the core material, ℓ_L and ℓ_C are those in the roll and in the crosswise direction, respectively. As the average flux density in the magnet core at the maximum excitation of the booster magnet is estimated to be about 16 kG, where $\mu_L \simeq 10{,}500$ and $\mu_C \simeq 300$, the drop of the magnetomotive forces in the magnet core is determined

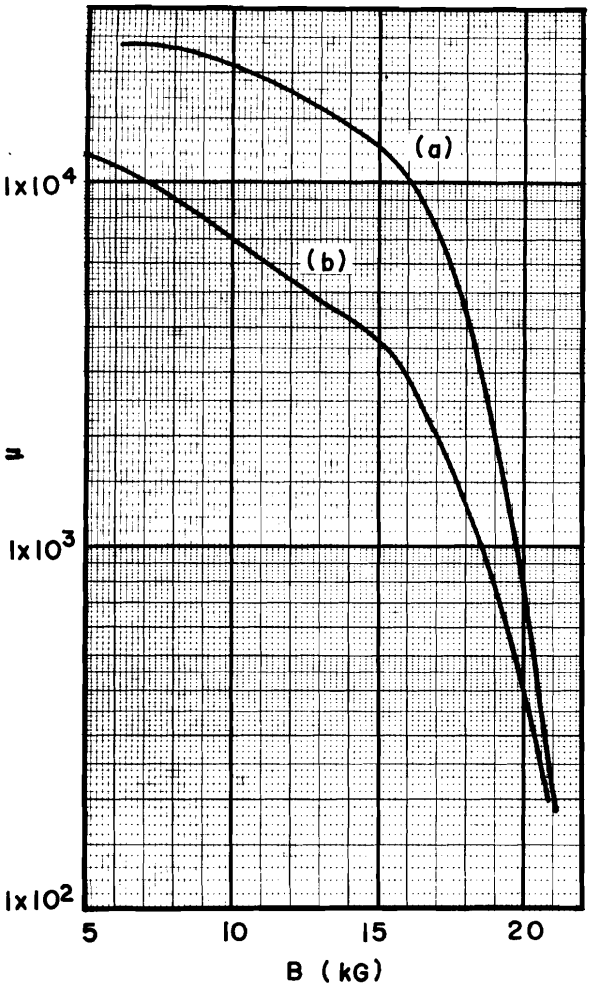

Fig.6. B-μ curves applied to the field calculations. (a) is the average B-μ curve of the oriented steel in the roll direction, and (b) the lower limit of the B-μ curve.

only by the contribution from the portion of the core in the crosswise direction. The drop amounts to 3.5 % of that dissipated in the magnet gap g for the designed geometry of the magnet $\ell/g \simeq 30$ and $\ell_L/\ell_C \simeq 1.5$. Then, we can expect that the fluctuation of the magneto-motive forces dissipated in the core, is 0.18 % in standard deviation, assuming random-shuffling of laminations.

Moreover, the vertical component of the magnetic field at any point on the median plane of the magnet gap comes mainly from the magnetization of the neighbouring laminations. Namely, the laminations within the range of the order of the magnet gap g along the central orbit, where 190 sheets of laminations are contained, are responsible for the central vertical field by 70 % of the field strength on the median plane. Therefore, fluctuation of the mmf drop in the magnet core among every 190-sheets groups almost determines the fluctuation of the central field, which is inversely proportional to the square root of the number of sheets contained in the range of g. By this collective effect of laminations, the statistical fluctuation of the central field damps at least by a factor of 20 from the mmf fluctuation in the laminations, and is expected to be one part of 10^4 in standard deviation. Such fluctuation of the magnetic field is one-third as much as the fluctuation required by the orbit analysis.

The statistical fluctuation of the coercive force

Another possibility of the field variation along the orbit is introduced into the injection stage by the statistical fluctuation of the coercive force. The injection field is designed a

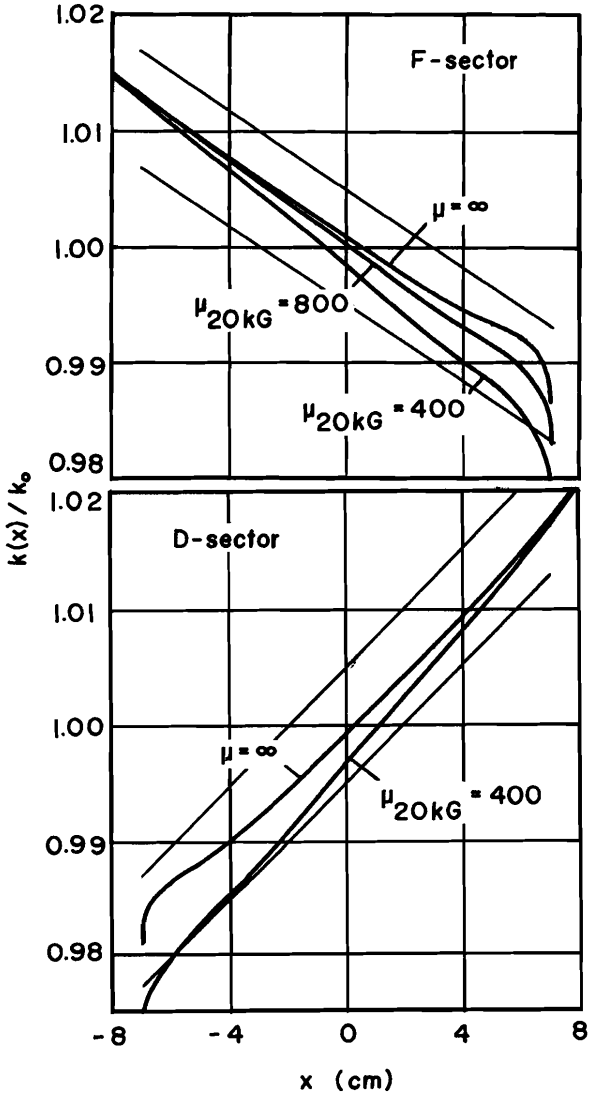

Fig.7. Field gradient distributions calculated by SIBYL program. Curves denoted by $\mu_{20kG} = 800$ and $\mu_{20kG} = 400$ are corresponding to those with B-μ curves (a) and (b) in Fig.6, respectively.

relatively high field of 2 kG. The coercive force of at most 0.6 oersted and the fluctuation of 10 % in standard deviation are expected for the supplied steel at the normal operation of 20 Hz. Owing to the collective effect of laminations, the remanent field fluctuation is estimated to be 0.1 gauss. Therefore, we can ignore the statistical fluctuation of the coercive forces, unless it is enhanced by a large mechanical stress introduced at the fabrication stage of the magnet blocks.[2]

VI. Iron loss of the magnet core

An iron loss of the booster magnet is of small amount in the total power consumption of the magnet or the resonant network involving the magnet system, as shown in Table 6. Therefore, the problems concerning with the iron loss in the core material are not those of the power supply, but of heating-up the core materials.

Table 6. Power consumption of the booster magnet

dc RI^2 loss	118.7 kW
ac RI^2 loss	28.8 kW
hysteresis loss	25.8 kW
iron eddy loss	2.1 kW
eddy current loss in copper conductor	19.2 kW

Fig.8 shows ac iron losses of the proposed oriented steel at 20 and 50 Hz in comparison with those of ordinary silicon steel. The losses of the oriented steel magnetized in the rolling and the crosswise direction lie in the intermediate region between the losses of the high- and low- grade silicon sheets. In spite of low specific resistance, it does not seem that the proposed steel is particularly inferior in the view point of the loss. The iron loss of the magnet unit at the normal operation is estimated to be 3.1 kW from the average minor loops in the parallel and crosswise magnetizations to the roll direction. In order to estimate the temperature rise of the magnet due to the iron loss, heat transmission coefficient at the surface of the magnet was measured with 1.3 GeV Electron Synchrotron magnet at Institute for Nuclear Study, University of Tokyo. The experimental results predict the maximum temperature rise of the booster magnet is 23°C without any special cooling device.

VII. Conclusions

The proposed low-carbon and low-silicon oriented steel is expected to be successfully applied to fast-cycling synchrotron magnets, particularly to the magnets of proton synchrotron, which do not associate with synchrotron radiation and are desirable to operate at higher fields in the view point of the construction costs. The mechanical properties of the material may require some additional cautions in the handling of the laminations compared with ordinary transformer sheets. The high field characteristics in the electro-magnetic properties of this material will fulfill our stringent requirements on the field qualities. It is desirable that the fluctuation of the electro-magnetic properties, particularly of the permeabilities at high field, is reduced to some extent, in order to assure a sufficiently small fluctuation of the peak field of the booster magnet.

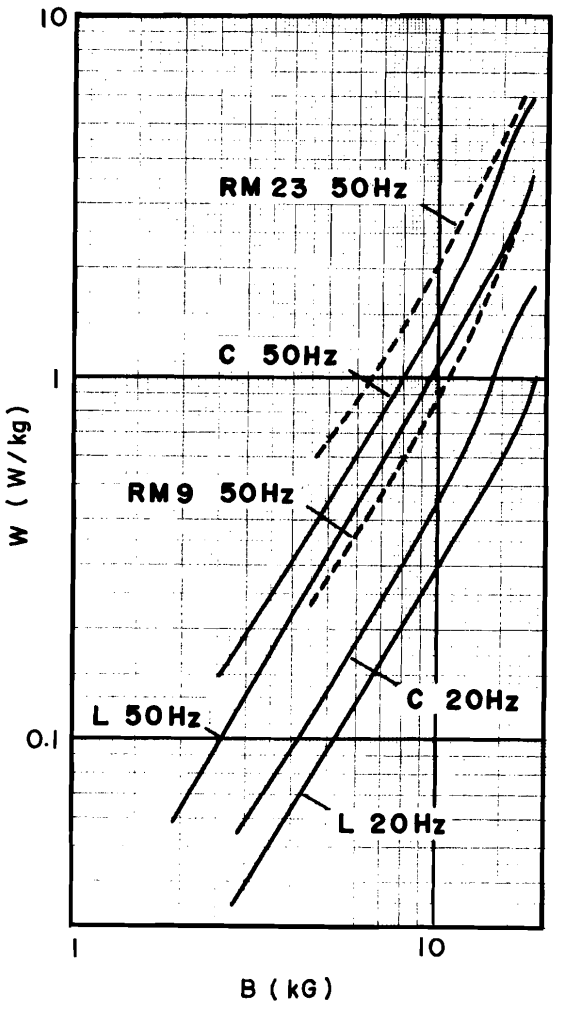

Fig.8. Iron loss of the oriented steel and ordinary silicon steel RM9 and RM23.

The cost of the present material is mostly determined by the complexity at the sequence of the production processes. This fact suggests the cost of the material is the same as that of high-grade silicon steel.

The future improvements of the proposed oriented steel seem to promise bright prospects. For instance, it will be technically feasible without great difficulty that an oriented steel, whose average permeability at 20 kG is as high as 1,200 in the roll direction, is in mass-production. Another possibility of the future development of the fast-cycling magnet is the application of cube-oriented steel, which has no direction of difficult magnetization in the rolling plane. In the present stage, however, such a material has problems in mass-production and in cost.

The authors wish to express their gratitude to Drs. I. Goto and I. Matoba, Kawasaki Steel Corporation, for supplying the data on the electromagnetic properties of the oriented steel and for valuable advise on the application of the material to the magnet. They would like to thank Prof. T. Doke, Dr. M. Kihara and Mr. K. Endo for valuable discussions, and they also thank Prof. T. Nishikawa for his encouragement throughout this work.

References

1. T. Doke, T. Hirose, M. Kihara, H. Sasaki, and M. Masuda, Nucl. Instr. Methods 83, 300 (1970).

2. H. Sasaki, Nucl. Instr. Methods 14, 252 (1961).

3. M.G. White, F.C. Shoemaker, and G.K. O'Neill, Proc. CERN Symposium on High Energy Accelerators, Vol. 1 (1956), p. 525.

4. Private communication. The tensor treatments of the permeability in calculation program are undertaken by Mr. K. Endo, National Laboratory for High Energy Physics, Japan.